Properties of hexagonal polytypes of group-IV elements from first-principles calculations

C. Raffy, J. Furthmüller, and F. Bechstedt
Institut für Festkörpertheorie und Theoretische Optik, Friedrich-Schiller-Universität, 07743 Jena, Germany
(Received 27 March 2002; published 2 August 2002)

Results of *ab initio* calculations are reported for hexagonal polytypes of C, Si, and Ge in equilibrium and under hydrostatic pressure. For each polytype $2H$, $3C$, $4H$, and $6H$, the atomic geometry, the energetics, and the electronic structure are studied. The resulting lattice parameters are in good agreement with measured values. While $3C$ is the most stable polytype for each element, pressure-induced phase transitions to hexagonal modifications are found to be possible. Silicon is the most favorable candidate in this respect. The results are interpreted within the axial next-nearest-neighbor Ising model. It simultaneously allows the derivation of formation energies for stacking faults in agreement with other calculations and measurements. We predict significant differences in the band structures between the hexagonal polytypes and the diamond structure. This holds especially for the energy gaps and the location of the conduction-band minima. Trends with the hexagonality of the polytype and the element are derived.

DOI: 10.1103/PhysRevB.66.075201 PACS number(s): 61.50.Ks, 61.66.Bi, 71.20.Nr

I. INTRODUCTION

The group-IV elements silicon (Si) and germanium (Ge) usually crystallize in the cubic diamond structure, in which the atoms are fourfold coordinated. The nearest-neighbor atoms form regular tetrahedra. The bonding configuration is mainly characterized by sp^3 hybrids. At high pressure, however, several polymorphs with varying coordination have been reported.[1–6] Carbon (C) also exhibits a number of polymorphs.[7,8] Besides the cubic diamond structure, graphite and crystalline structures of C_{60} molecules are, for instance, observed.

Polytypism is a one-dimensional variant of the phenomenon of polymorphism. In group-IV materials, polytypes of the common diamond structure can be formed by keeping the tetrahedral coordination, but varying the stacking sequence along one direction.[9] The polytypes differ only in the manner in which the bilayers are stacked along the hexagonal *c*-axis direction, either in the ''chair'' or in the ''boat'' conformation (see Fig. 1). The first case corresponds to a pure cubic (C) stacking of the IV-IV double layers in the [111] direction. The bonds nonparallel to [111] do not change their orientation, and the periodicity in the [111] direction is reached after three bilayers. The diamond structure is thus called $3C$ in Ramsdell notation.[10] In the ''boat'' conformation, pure hexagonal (H) stacking occurs in the [0001] direction. The orientation of the bonds nonparallel to [0001] is changed in every bilayer. Periodicity occurs after two IV-IV bilayers. The resulting wurtzite structure is thus called $2H$. It is sometimes also referred to as lonsdaleite, or hexagonal diamond. Other polytypes represent hexagonal (H) or rhombohedral (R) combinations of these stacking sequences.[9] Important examples are the $4H$ and $6H$ polytypes with four or six bilayers and, hence, eight or 12 atoms in the corresponding hexagonal unit cell. The $3C$, $2H$, $4H$, and $6H$ structures are represented in Fig. 1. Many other polytypes, with larger unit cells, are possible. In the case of the only stable group-IV compound SiC, more than 200 polytypes have been determined.[11]

Under extensive pressure and heat treatment, the transformation of cubic-diamond silicon crystals into wurtzite Si was already observed 40 years ago.[12] The generation of hexagonal phases of Si during high-temperature indentation of diamond-structure Si crystals was first studied by Eremenko and Nikitenko.[13] The transformation mechanism in the process of plastic deformation has then been studied in detail by Pirouz *et al.*[14] Tan *et al.* have also observed the formation of $2H$-Si in ion-implanted diamond-structure crystals.[15] More recently, hexagonal Si has been prepared by pulsed laser beam annealing,[16] by laser ablation,[17] and by the cluster-beam evaporation technique.[18] Moreover, poly-Si layers fabricated routinely by low-pressure chemical vapor deposition (CVD) show, besides $2H$,[19] other higher-order polytypes like $4H$ and $9R$.[20]

The generation of a hexagonal polytype after temperature indentation works for germanium as well. As for Si, ribbons of wurtzite Ge have been obtained in a diamond-structure matrix.[21–23] Interestingly, Ge nanocrystallites embedded in $4H$-SiC matrices with diameters below 10 nm also exhibit

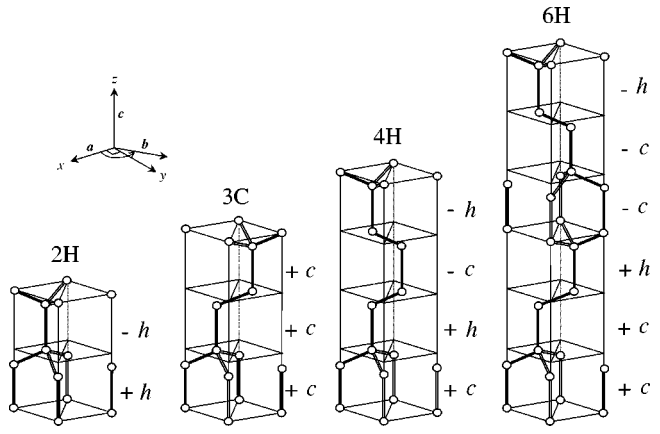

FIG. 1. The bond stacking in [0001] direction in the four polytypes studied. The hexagonal unit cells are shown. Bonds in a $(11\bar{2}0)$ plane are indicated by heavy solid lines. The cubic (c) or hexagonal (h) character of a bilayer is defined by the nonparallel bond in this plane. The signs + and − denote the orientation of a bilayer.

hexagonal crystal structures.[24,25] They have been prepared by ion implantation and subsequent rapid thermal annealing. Furthermore, 4*H*-Ge could be obtained by annealing the ''allo-germanium'' phase.[26]

The hexagonal wurtzite polytype of carbon was first found in meteorites.[27] It was then synthesized in the laboratory by Bundy and Kasper from graphite, using extreme conditions of pressure and temperature.[28] In diamond-like-carbon films grown by CVD, a high density of (111) microtwins and stacking faults has been observed, indicating that part of the deposited films might contain the hexagonal diamond phase.[29] Homogeneous nucleation of diamond powder has been studied in a low-pressure microwave-plasma reactor.[30] The powder was identified to be a mixture of carbon polytypes with 3*C*, 2*H*, and 6*H* parts. Diamond polytype films (mainly 4*H*) were deposited by pulsed-laser-induced reactive quenching.[31] Hexagonal diamond has been also observed during pulsed-laser-induced transformation of hexagonal graphite.[32]

Though the 2*H*, 4*H*, and 6*H* polytypes of the three elements have been observed experimentally, little is known of their structural, cohesive, and electronic properties as well as their stabilities relative to the parent cubic structure. The lattice constants of 2*H*-Si (Refs. 13,17,19 and 33), 2*H*-Ge (Ref. 21), 2*H*-C (Ref. 28), and 4*H*-C (Ref. 31) have been determined using x-ray diffraction or high-resolution transmission electron microscopy (TEM). The Raman spectra of wurtzite silicon (Ref. 34) and 4*H*-Ge (Ref. 26) have been reported. A detailed symmetry analysis of the infrared- and Raman-active vibrational modes[7] has been published for a series of carbon polytype structures. The lattice constants and the electronic structures have been studied theoretically for the 2*H* (Ref. 35) and 4*H* (Ref. 31) polytypes of carbon within the framework of the density functional theory[36] (DFT) and the local density approximation[37] (LDA), using the linear muffin-tin orbital (LMTO) method together with the atomic-sphere approximation (ASA). Calculations of the electronic properties of wurtzite Si and Ge within the empirical pseudopotential method have been reported.[38] *Ab initio* pseudopotentials have been used to study the band structures of 2*H*-Si and 2*H*-C (Ref. 39) and their energetics (Ref. 40).

In this paper, we present results of comprehensive DFT-LDA studies of the 2*H*, 3*C*, 4*H*, and 6*H* polytypes for the group-IV elements C, Si, and Ge. We discuss their atomic structure, their energetical stability, possible pressure-induced phase transformations, and their electronic band structure. The relative energies are used to derive the parameters of an axial next-nearest-neighbor Ising (ANNNI) model.[41] This model is used to discuss trends in energetical stability and the probability to observe two-dimensional defects like stacking faults.

II. COMPUTATIONAL METHODS

Our calculations are based on the DFT-LDA.[36,37] The Vienna Ab-initio Simulation Package (VASP) (Ref. 42) is used. The potential energy of an electron in the field of the nuclei screened by the core electrons is represented by non-norm-conserving ultrasoft pseudopotentials.[43] This allows a substantial softening of the potential, even for the first-row element C which has no core *p* electrons. In Ge, the 3*d* electrons are treated as core electrons. However, non-linear core corrections[44] are taken into account. The single-particle wave functions are expanded into a plane-wave basis set. The kinetic-energy cutoffs considered are 24.2, 16.1, and 10.4 Ry for C, Si, and Ge, respectively. The electron-electron interaction is described by the Ceperley-Alder functional as parametrized by Perdew and Zunger.[45]

The **k**-space integrals, which appear in the expression of the total energy and the electron density, are replaced by sums over special points generated by the Monkhorst-Pack method.[46] The four polytypes 2*H*, 3*C*, 4*H*, and 6*H* considered in Fig. 1 are represented in nH unit cells ($n=2,3,4,6$) containing n IV-IV pairs, with the lattice constants a and c. They are primitive cells with the exception of the cubic case. As an advantage, a hexagonal Brillouin zone (BZ) with nearly the same basis area, but a varying height $2\pi/c$, can be considered for all polytypes. We use approximately the same density of **k** points for all polytypes. A $11\times11\times k$ mesh guarantees the convergence, with k being an integer varying between 7 (2*H*), 5 (3*C*), 4 (4*H*), and 3 (6*H*). To check the energetical differences between the polytypes, the total energy calculations have been repeated for a representation of all polytypes in a 12*H* unit cell and a **k**-point mesh $11\times11\times2$.

For each polytype, we perform a full optimization of the atomic structure. In the 3*C* case, only the lattice constant a has to be varied, since the constant c is fixed by the ideal ratio $c/(3a)=\sqrt{2/3}=0.8165$. For the hexagonal polytypes, besides a and c, one has to determine the $(n-1)$ internal-cell parameters $\delta(i)$ and $\varepsilon(i)$.[47,48] For a given volume of the unit cell, a and c are determined in such a way that the total energy becomes a minimum. For a given pair (a,c), the $(n-1)$ internal degrees of freedom are varied until the forces on the atoms vanish. The data of total energy versus volume are fitted using the Vinet equation of state.[49] This equation has been found to be quite accurate for many crystals under compression and for hexagonal polytypes too.[50] Besides the equilibrium volume, the fit gives the minimum total energy E_0, the isothermal bulk modulus B_0, and its pressure derivative B_0' at the equilibrium.

III. RESULTS

A. Structural properties

The results of the structural optimizations are listed in Table I for the four polytypes and the three group-IV elements under consideration. The polytypes are ordered according to their hexagonality, defined by the ratio of the number of the hexagonal bilayers to the total number of bilayers per unit cell (cf. Fig. 1). Between the most extreme polytypes 3*C* with $h=0\%$ and 2*H* with $h=100\%$, one finds the intermediate polytypes 6*H* with $h=33\%$ and 4*H* with $h=50\%$. Apart from the chemical trend with the group-IV element, the results show clear trends with the hexagonality. For all elements, the lattice constant a decreases, whereas the normalized lattice constant c/n and the ratio $c/(na)$ increase

TABLE I. Calculated equilibrium structural parameters and total energies relative to the $3C$ value. For comparison other experimental and theoretical values are also given.

Element	Polytype		a (Å)	c/n (Å)	$c/(na)$	B_0 (kbar)	B_0'	E_0 (meV/atom)
C	$3C$	present	2.495	2.0347	0.8165	4713	3.73	0
		expt. [a]	2.522	2.059	0.8165	4420		
	$6H$	present	2.490	2.047	0.8221	4712	3.74	5.9
	$4H$	present	2.488	2.052	0.8248	4687	3.92	9.2
		calc. [b]	2.5221	2.0593	0.8165			
		expt. [c]	2.522	2.0585	0.8162			
	$2H$	present	2.481	2.066	0.8327	4743	3.65	25.3
		calc. [d]	2.50	2.070	0.828	4400	3.5	30.0
		calc. [e]	2.49	2.072	0.8325			25.3
		expt. [f]	2.52	2.06	0.8175			
Si	$3C$	present	3.816	3.115	0.8165	966	4.18	0
		expt. [a]	3.8403	3.136	0.8165	979	4.24	
	$6H$	present	3.810	3.122	0.8195	967	4.13	1.0
	$4H$	present	3.806	3.127	0.8215	967	4.13	2.4
	$2H$	present	3.798	3.140	0.8267	967	4.06	10.7
		calc. [e]	3.800	3.135	0.8250			11.7
		expt. [g]	3.86	3.155	0.817			
		expt. [h]	3.837	3.158	0.823			
		expt. [i]	3.84	3.140	0.815			
		expt. [j]	3.84	3.090	0.8165			
Ge	$3C$	present	3.979	3.248	0.8165	725	4.80	0
		expt. [a]	4.001	3.267	0.8165	770	4.6	
	$6H$	present	3.972	3.255	0.8196	728	4.77	4.3
	$4H$	present	3.969	3.258	0.8208	728	4.77	6.9
	$2H$	present	3.962	3.269	0.8250	728	4.74	16.1
		calc. [k]						15
		expt. [l]	3.96	3.285	0.8295			

[a]Reference 51.
[b]Reference 8 (data calculated from computer simulation of x-ray diffraction patterns).
[c]Reference 31.
[d]Reference 52.
[e]Reference 40.
[f]Reference 28.
[g]Reference 13.
[h]Reference 33.
[i]Reference 17.
[j]Reference 19.
[k]Reference 2.
[l]Reference 21.

with increasing hexagonality. These trends correspond to an increasing deformation of the bonding tetrahedra, which are stretched along the c axis. This is in agreement with other calculations and, in principle, also with measurements (see Table I). However, systematic experimental studies are missing because of sample-quality problems. Of course, the theoretical lattice constants are slightly smaller than the experimental ones due to the overbinding tendency within the DFT-LDA.[53] Interestingly, the trends are the same as in the case of the SiC polytypes,[47] in spite of the modifications due to the partially ionic bonding in the compound. For all hexagonal polytypes, the ratio $c/(na)$ is larger than the ideal value $\sqrt{2/3}$ valid for $3C$. This agrees with tendencies observed for III-V and II-VI compounds which crystallize normally within the zinc-blende structure. In contrast, the compounds for which the wurtzite polytype is more stable, exhibit a $c/(na)$ ratio below the ideal value.[40]

The overall elastic properties are represented by the isothermal bulk modulus and its pressure derivative. The calculated values in Table I confirm the result already observed that the bulk modulus is rather insensitive with respect to a certain polytype structure.[47,54] Only in the carbon case does there seem to be a weak variation influenced by two opposite tendencies. The $4H$ polytype, with a hexagonality $h=50\%$, possesses the smallest bulk modulus.

The atomic relaxations, representing the deviations of the atomic positions from the ideal tetrahedron structure, are listed in Table II. Although they are extremely small, they might be important for the stabilization of the polytypes.[47,48,55] This is well known from SiC, for which similar absolute values of the relaxations have been derived, even if the signs of $\varepsilon(1)(2H)$, $\delta(2)(4H)$, and $\delta(3)(6H)$ are different. However, in the case of C, Si, and Ge, we have checked that the relaxations do not result in a change fo the

TABLE II. Internal-cell geometry parameters. For definitions, see Refs. 47 and 48.

Element	Polytype	i	$10^4\times\varepsilon(i)$	$10^4\times\delta(i)$
C	$2H$	1	−6.9	–
	$4H$	1	14.0	–
		2	−1.1	15.1
	$6H$	1	12.7	–
		2	7.0	14.0
		3	−1.3	5.7
Si	$2H$	1	−9.4	–
	$4H$	1	6.6	–
		2	−1.9	8.5
	$6H$	1	6.6	–
		2	3.6	7.8
		3	−1.2	2.9
Ge	$2H$	1	−7.0	–
	$4H$	1	8.0	–
		2	−1.7	9.7
	$6H$	1	7.1	–
		2	4.0	8.5
		3	−1.4	3.1

stability ordering of the polytypes. Their values can be compared with other calculations or measurements only in the case of 2H. Yeh *et al.*[40] found, with $\varepsilon(1)=-0.001$, practically identical values for C and Si.

B. Energetical stability and stability against pressure

The ground-state energies of the hexagonal polytypes with respect to the diamond polytype are given in Table I. The cubic polytype is the most stable one, followed by $6H$ and $4H$. The energy of the wurtzite phase is substantially higher. There is a pronounced increase of the energy with the hexagonality. Our results for the $2H$-$3C$ energy differences for C and Si agree well with other calculations, especially with those by Yeh *et al.*,[40] in which norm-conserving pseudopotentials have been used. For Si, the energies of the polytypes $3C$, $6H$, and $4H$ are very close to each other, which may indicate good chances for the preparation of

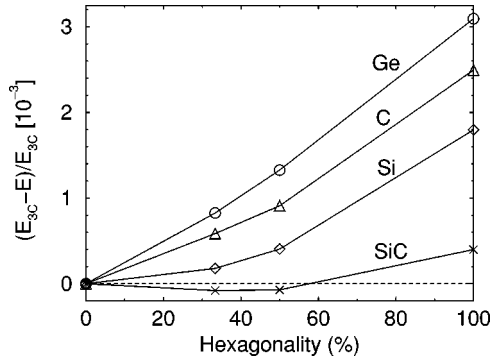

FIG. 2. Relative energy vs hexagonality of the polytype. The reference value $E_0(3C)$ corresponds to the negative cohesive energy within DFT-LDA.

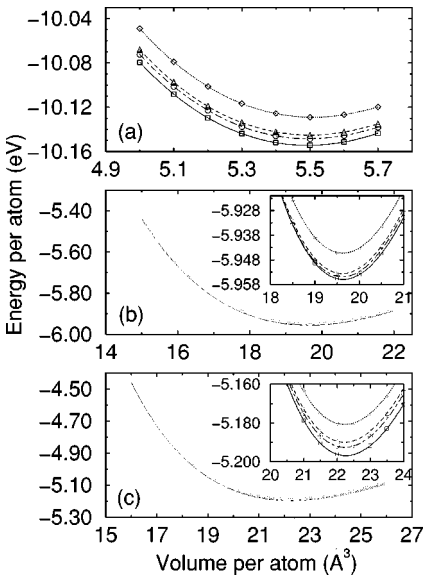

FIG. 3. Total energy vs volume for different polytypes. (a) C, (b) Si, and (c) Ge. $3C$: squares, solid lines. $6H$: circles, dot-dashed lines. $4H$: triangles, dashed lines. $2H$: diamonds, dotted lines.

polytypes with $h\lesssim 50\%$. Figure 2 shows the relative energies of the polytypes as a function of hexagonality. For comparison, the values for SiC polytypes are also given.[56] For SiC, a minimum is observed, due to the fact that $6H$ and $4H$ are more stable than $3C$. In contrast, the curves for C, Si, and Ge exhibit a monotonous increase. However, the chemical trend is very interesting and somewhat surprising. One observes the ordering Ge, C, Si which contradicts the ordering of bond energies of the diamond structures $E_0(3C)=-10.147$ (C), -5.957 (Si), and -5.195 (Ge) eV/atom. This has consequences for the probability to prepare hexagonal polytypes and to find stacking faults in the diamond-structure crystals. From a thermodynamical point of view, the tendency to the formation of hexagonal structures is much more pronounced for Si in comparison to Ge. Carbon takes an intermediate position.

Strain may play an important role in the formation of hexagonal polytypes of group-IV elements.[12–15,22,28] For that reason, the volume dependence of the total energies is plotted in Fig. 3. The curves indicate the energetical ordering of the polytypes discussed above at the equilibrium. However, for smaller volumes, i.e., when a hydrostatic pressure is applied, phase transitions can occur between Si and Ge polytypes. This is better seen when considering the variation of the enthalpy. For a given volume, the pressure is derived from the Vinet equation of state. This allows us to represent the enthalpy $H=E+pV$ as a function of pressure in Fig. 4. The enthalpies of the four polytypes considered for Si and Ge get closer and closer with increasing pressure. According to Fig. 4, phase transitions may occur between $3C$ and $6H$ (at about 100 kbar for Si and 250 kbar for Ge) and between $6H$ and $4H$ (at about 450 kbar for Si and a pressure above 500 kbar for Ge). However, the many experimental and theoretical studies devoted to the understanding of the high-pressure polymorphism of the elemental semiconductors Si and Ge have shown that phase transformations into nontet-

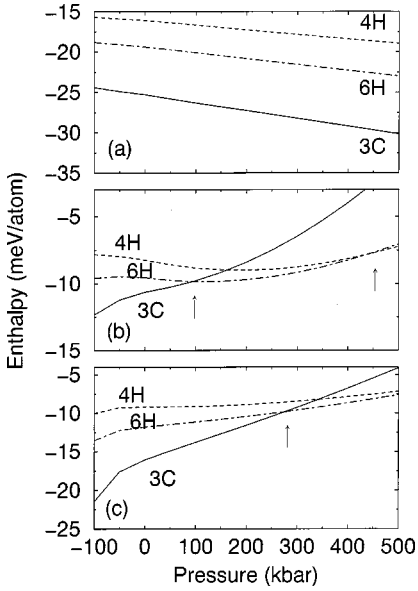

FIG. 4. Enthalpy as a function of pressure for polytypes of C (a), Si (b), and Ge (c). The enthalpy of $2H$ is taken as reference. Transition pressures are indicated.

rahedrally coordinated polymorphs can occur at lower transition pressures.[1–6] The cubic diamond phase of Si transforms into the metallic β-tin phase (body-centered-tetragonal) at 78 kbar,[3] then into an intermediate orthorhombic $Imma$ phase, and into a simple hexagonal structure. The same sequence is found for germanium.[4–6] Under depressurization, the β-tin phase can generate complex metastable phases like r8 (rhombohedral), st12 (simple tetragonal), bc8 (body-centered-cubic), or amorphous phases.[57–59] For carbon, in contrast to Si and Ge, the $3C$ polytype remains stable even at high pressure, as indicated in Fig. 4(a). Phase transformations, which require bond breaking and rebonding, are hindered by the large C-C bond energy.

C. ANNNI model and stacking-fault formation

The polytypes differ only in the stacking sequence of the tetrahedra along the [0001] direction. The resulting energetical differences due to this uniaxial character can be reasonably described by a one-dimensional Ising-type model, the ANNNI model.[41,48,60,61] In this model, each bilayer i is characterized by a spin variable $\sigma_i = \pm 1$ according to the orientation of the bonding tetrahedra. These orientations are indicated in Fig. 1. The ANNNI model is usually applied to the total energies. Here, we generalize the model to the enthalpies, i.e., to the situation in the presence of a finite hydrostatic pressure. The enthalpy per two atoms can be described as

$$H(p) = H_0(p) - \frac{1}{n}\sum_{i=1}^{n}\sum_{j=1}^{\infty} J_j(p)\sigma_i\sigma_{i+j}, \qquad (1)$$

where the label i counts the bilayers in the unit cell of the nH polytype and j runs over all interacting bilayers. More complicated interactions, such as four-spin correlations,[60,61] have been neglected. The parameters $J_j(p)$ are the interaction energies with the jth-neighbor bilayer in the presence of a hydrostatic pressure p. The largest term $H_0(p)$ in Eq. (1) represents the enthalpy of one bilayer in a polytype without interaction between the bilayers. Assuming that the long-range interactions are small, we restrict the j sum up to the third neighbors ($j \leqslant 3$).

The values J_1, J_2, and J_3 are derived from the calculated total energies (cf. Table I and Fig. 3). They are listed in Table III for the equilibrium state ($p=0$) and for a certain hydrostatic pressure ($p=400$ kbar). For each element at zero

TABLE III. Parameters of the ANNNI model (in meV per pair) and resulting stacking-fault energies (in mJ/m^2). Besides the zero-pressure results, high-pressure ones (taken at $p=400$ kbar) are given in parentheses.

Element		J_1	J_2	J_3	γ_{ISF}	γ_{ESF}	γ_{TSF}
Ge	present	16.5 (8.5)	-1.2 (-4.5)	-0.46 (-1.74)	69.7 (12.8)	62.2 (-22.5)	30.0 (-16.2)
Si	present	11.4 (6.2)	-2.9 (-6.2)	-0.75 (-2.3)	39.3 (-13.2)	20.6 (-63.9)	8.4 (-38.7)
	calc. [a]				38	20	
	calc. [b]				33	26	
	calc. [c]				47	36	
	calc. [d]				64	44	19
	calc. [e]				87.7	70.8	33.8
	expt. [f]				69	60	
C	present	25.6 (29.6)	-3.4 (-3.8)	-0.35 (-0.43)	259.7 (316.8)	214.5 (263.8)	105.2 (129.2)
	calc. [a]				318	254	
	calc. [b]				300	253	
	expt. [g]				279 ± 41	279 ± 41	

[a]Reference 65.
[b]Reference 63.
[c]Reference 62.
[d]Reference 66.
[e]Reference 64.
[f]Reference 67.
[g]Reference 68. ISF and ESF have not been distinguished.

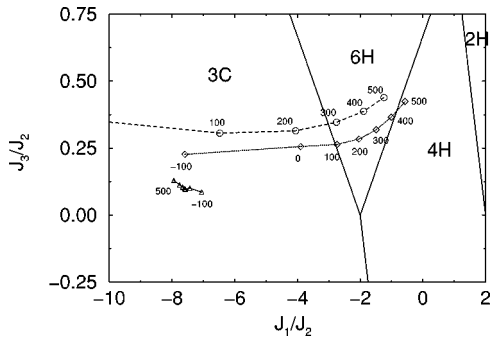

FIG. 5. Phase diagram of the four polytypes $2H$, $3C$, $4H$, and $6H$ within the ANNNI model. The circles (Ge), diamonds (Si), and triangles (C) indicate the group-IV element. The pressure values are given in kbar.

pressure, J_1 is positive and much larger than $|J_2|$ and, all the more, than $|J_3|$. This indicates a stabilization of the polytype constituted by bilayers with the same spin ($\sigma_i\sigma_{i+1}>0$ for all i). According to the total-energy differences $2J_1+2J_3$ ($2H$), $J_1+2J_2+J_3$ ($4H$), and $2(J_1+2J_2+3J_3)/3$ ($6H$) with respect to the $3C$ polytype,[48,62] this is a consequence of the fact that $3C$ is the most stable polytype at zero pressure. For Si and Ge, when a hydrostatic pressure is applied, J_1 decreases whereas $|J_2|$ increases. Approximately for $2|J_2|/J_1>1$ (if J_3 is neglected), the $4H$ and $6H$ polytypes are more stable than $3C$. For a huge pressure of 400 kbar, this is clearly the case. Hydrostatic pressure weakens the effective first-nearest-neighbor interaction and increases the interaction with more distant bilayers, resulting in a stabilization of the hexagonal structures. This is shown in the phase diagram in Fig. 5, which contains a triple point for $J_3=0$ and $J_1=-2J_2$ at which the $3C$, $6H$, and $4H$ phases degenerate. The situation is completely different for carbon. Both J_1 and $|J_2|$ increase with increasing pressure. As indicated in Fig. 5, this behavior stabilizes the cubic phase. The triangles representing carbon in the phase diagram even move more into the $3C$ domain away from the $6H$ and $4H$ domains.

Besides the polytypism, the ANNNI model also enables one to discuss some two-dimensional defects in cubic crystals, like the stacking faults. The most common stacking faults are the intrinsic stacking fault (ISF), the extrinsic stacking fault (ESF), and the twin stacking fault (TSF).[62–66] The ISF and ESF are related to the bond tetrahedron rotation in two bilayers and differ by the distance of the two perturbed bilayers by one or two bilayers. The ISF can be thought of as removing one bilayer from the infinite $3C$ stacking sequence. Instead, the ESF can be thought of as adding one bilayer to the stacking sequence. The TSF is defined by a reflection symmetry with respect to a plane midway between a bilayer. The formation energy E_f of a stacking fault per two-dimensional unit cell perpendicular to the stacking direction, is given within the ANNNI model by[62,65]

$$E_f(\mathrm{ISF})=4(J_1+J_2+J_3),$$
$$E_f(\mathrm{ESF})=4(J_1+2J_2+2J_3), \qquad (2)$$
$$E_f(\mathrm{TSF})=2(J_1+2J_2+3J_3).$$

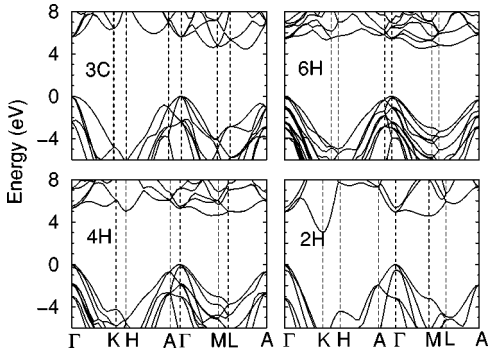

FIG. 6. Band structures of hexagonal C polytypes.

The stacking fault energies γ(ISF/ESF/TSF) per unit area follow from the values (2) by division with the area $\sqrt{3}a^2/2$ of one atom in a (111) plane. These values are listed in Table III together with results of other calculations[62–66] and measurements.[67,68] The values confirm again that there is no chemical trend along the row C, Si, Ge. From a thermodynamical point of view, it is much easier to generate stacking faults in Si crystals than in Ge ones. Their creation costs a lot of energy in diamond crystals. In strained Si and Ge crystals, the probability for the generation of stacking faults is increased, whereas it is more difficult to create such perturbations in strained diamond crystals. In pulsed-laser-beam crystallized Si thin films, indeed many extrinsic stacking faults have been observed.[16]

While no chemical trend is observed in Table III, the formation energies at zero pressure are reduced along ISF, ESF, TSF, i.e., with increasing the distance of the rotated tetrahedra within the stacking faults. While the TSF is the most favorable fault at the equilibrium, the ESF takes over this role under hydrostatic pressure, at least for Si and Ge. The agreement with the ISF and ESF energy values obtained within *ab initio* plane-wave pseudopotential calculations[62,63,65] is excellent, considering the numerical accuracy requirements. The agreement with the experimental data is also good, in particular for diamond.[68] For silicon, the energetical ordering of the faults is the same. The absolute experimental values[67,68] are larger than the computed ones. However, one has to take into acount the complicated procedure to extract such energies from measurements.

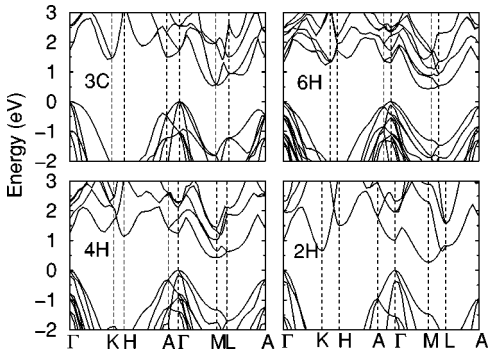

FIG. 7. Band structures of hexagonal Si polytypes.

D. Band structures and their pressure dependences

The electronic band structures of the four polytypes of C, Si, and Ge under consideration are plotted in Figs. 6, 7, and 8. They are calculated in DFT-LDA for the structural parameters obtained in Sec. III A. The eigenvalues of the Kohn-Sham equation have been computed for **k** points along high-symmetry lines of the corresponding hexagonal BZ. For direct comparison, the cubic structures are represented in a hexagonal cell. The size of the different BZ's parallel to the *c* axis varies with the polytype, whereas all lengths perpendicular to the *c* axis are practically equal. Nevertheless, in Figs. 6, 7, and 8, with a view to the presentation, we use the same extent of the *x* axis and correspondingly rescale all segments. We do not consider any quasiparticle corrections to account for the excitation aspect.[69,70] The band structures thus suffer from the well-known band gap underestimate of the DFT-LDA.

Two principal effects of the polytypism are represented in Figs. 6, 7, and 8. (i) The varying extent of the unit cells in the direction of the *c* axis gives rise to an inverse variation of the BZ in this direction. Consequently, one important effect is related to the folding of the bands parallel to ΓA, HK, and LM directions. (ii) Besides the translational symmetry, the scattering properties of the atomic arrangements also change with the polytype. Overall features of the band structures of the three hexagonal polytypes agree for symmetry reasons. Bands versus the lines AH and AL on the surface and the bottom of the BZ are twofold degenerate in crystals with C_{6v}^4 symmetry. This is due to the presence of a sixfold screw axis along [0001] and time-reversal symmetry.[71]

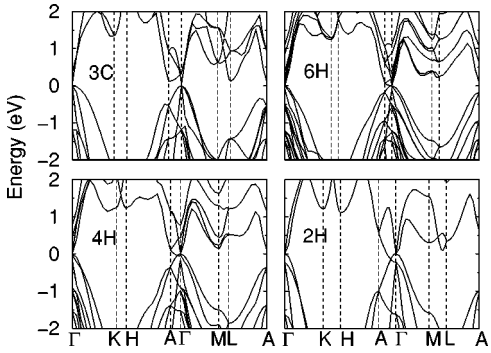

FIG. 8. Band structures of hexagonal Ge polytypes.

The band structures of C and Si (Figs. 6 and 7) are rather similar. Independent of the polytype, they represent indirect semiconductors. The lowest conduction-band minimum occurs close to the M point on the Σ line, except for $2H$-C (minimum at K) and $3C$-C. For $3C$-C, the minimum lies between L and A, and is only slightly below the minimum on the Σ line. For the other polytypes, the deviation from the M position holds in particular for Si, because in the diamond structure the lowest conduction-band minimum occurs on the ΓX line near X in the fcc BZ. For the wurtzite polytype, a pronounced minimum occurs at the K point. In $2H$ carbon, it is even below the other minimum, as also found for SiC.[72,73] For $4H$ and $6H$, the energetical distance of the valence and

TABLE IV. DFT-LDA energy gaps (first value, in eV) and their pressure coefficients (second value in meV/kbar). In addition, the crystal-field splitting Δ_{cr} (in meV) of the valence-band maximum and the valence-band discontinuities ΔE_v (in meV) with respect to the $3C$ polytype are given. The valence-band maximum is fixed at Γ. Three different conduction-band minima at Γ, near M (on the ΓM line), and near K (on the ΓK line) have been considered (cf. Figs. 6, 7, and 8). In a few cases, values from other DFT-LDA calculations (Refs. 35,39, and 52) are given in parentheses.

Element	Polytype	Γ		M		K		Δ_{cr}	ΔE_v
C	$3C$	5.61	0.51	4.61	0.45	6.29	0.57	0	0
		(5.5[a], 5.57[b])		(3.8[a], 4.50[b], 4.3[c])	(0.6[c])				
	$6H$	5.40	0.40	4.51	0.51	5.90	0.04	163	143
	$4H$	5.31	0.35	4.62	0.45	5.49	0.05	243	160
	$2H$	4.96	0.21	4.56	0.43	3.03	−0.79	522	231
		(4.0[a], 4.67[b])		(3.98[b])		(2.7[a], 3.02[b], 3.3[c])	(−1.2[c])		
Si	$3C$	1.73	2.20	0.54	−1.39	1.42	−0.88	0	0
		(2.56[b])		(0.36[b])					
	$6H$	1.32	2.25	0.44	−1.46	1.24	−1.50	112	135
	$4H$	1.26	2.20	0.43	−1.52	1.26	−1.40	170	157
	$2H$	1.00	1.87	0.27	−1.75	0.64	−3.29	364	235
		(0.88[b])		(0.29[b])		(0.76[b])			
Ge	$3C$	0.04	3.04	0.57	−1.36	1.34	−0.54	0	0
	$6H$	0.00	2.31	0.27	−0.91	1.25	−1.09	101	112
	$4H$	−0.02	2.31	0.14	1.94	1.15	0.33	168	124
	$2H$	−0.13	1.92	0.30	−1.48	1.20	−3.45	-	138

[a]Reference 35.
[b]Reference 39.
[c]Reference 52.

conduction bands near K are seemingly increased. This can be explained by simplifying folding arguments. Going from $2H$ to $4H$ or $6H$ the point H (L) maps onto K (M) or onto $\frac{2}{3}HK$ ($\frac{2}{3}LM$). This folding is accompanied by a stronger interaction of the bands with partially the same *s*- and *p*-orbital character, which pushes the conduction-band minimum of $2H$ away from the valence bands. Then, the states near the LM line or ΓM line around M form the lowest conduction-band minimum of $4H$ and $6H$. For Ge, the interpretation of the band structure in Fig. 8 is more complicated. This is due to the numerical treatment of Ge in the DFT-LDA approach, which already gives an almost vanishing direct gap at Γ, and an almost vanishing indirect gap at L, for the diamond structure in the fcc BZ. Moreover, the DFT-LDA description does not give an indirect semiconductor, since the conduction-band minimum at L (fcc) is found to be slightly higher in energy than the one at Γ (fcc). As a consequence, the ''conduction bands'' and ''valence bands'' overlap energetically somewhat, with rising hexagonality. Then, $6H$-Ge possesses the character of a zero-gap semiconductor, whereas $4H$ and $2H$ get a weak metallic character. This metallic character is in contrast with the results of empirical-pseudopotential calculations,[38] which suggest a semiconducting character for $2H$-Ge. Another interesting fact is that for $3C$-Ge, the second smallest energy gap is located at the L point, which does not correspond to a band minimum for C and Si.

Values for important energy gaps E_g of the hexagonal polytypes are listed in Table IV together with their pressure coefficients $dE_g/dp|_{p=0}$. Using the bulk moduli B_0 given in Table I, the pressure coefficients can be immediately recalculated into the corresponding volume deformation potentials $a_v = -B_0 dE_g/dp|_{p=0}$. Three conduction-band minima are considered, at Γ, near M, and near K. Really the minima on the ΓK line near K and on the ΓM line near M have been considered. In the case of $2H$-C, $3C$-C, $2H$-Si, and $3C$-Si, the calculated gap energies agree well with the other *ab initio* pseudopotential plane-wave calculations[39] and also with the local-orbital method.[52] The values for $2H$-C and $3C$-C obtained within LMTO-ASA calculations[35] are somewhat smaller due to the influence of the atomic spheres chosen. For C and Si, we note the trend that all energy gaps decrease with the hexagonality. These findings are in clear contrast with the SiC polytypes, for which the fundamental gap increases with increasing hexagonality and approaches to the maximum value in the wurtzite structure.[72]

In the hexagonal nH polytypes, the threefold-degenerate valence-band maximum (VBM) of the $3C$ crystal splits into a twofold (p_x and p_y) Γ_{6v} VBM and a lower onefold (p_z) Γ_{1v} splitoff band. The splitting energy Δ_{cr} characterizes the crystal field, i.e., the deviations in the interaction of the atomic neighbors due to the changed geometry. The corresponding values of Δ_{cr} in Table IV increase dramatically with the hexagonality of the polytype. The increase is almost linear. Our values are in good agreement with other calculations for $2H$-C and -Si.[39]

The preparation of heteropolytypic structures, i.e., layered structures on the base of two polytypes (e.g., $3C$ and nH), opens new possibilities for applications of group-IV materials in novel electronic devices. The electronic structure of these heteropolytypic systems is governed by the valence-band discontinuity ΔE_v. We have calculated ΔE_v using the average local electrostatic potential as the reference level for the alignment. The influence of quasiparticle effects on the offsets is neglected. The valence-band discontinuities are found to be small. However, they also increase with the hexagonality. Together with the fundamental gaps in Table IV, one may also suggest small discontinuities for the conduction bands. It seems that the polytype combinations $3C/2H$ give rise to type-I heterostructures. This means both electrons and holes are localized in the regions of the hexagonal polytype. On the contrary, for the polytype combinations $3C/4H$ and $3C/6H$, we find a type-II behavior, with the electrons localized in the cubic region and the holes in the hexagonal region. We should mention that similar values of ΔE_v have been calculated by other authors for the $3C/2H$ combination of carbon and silicon.[39]

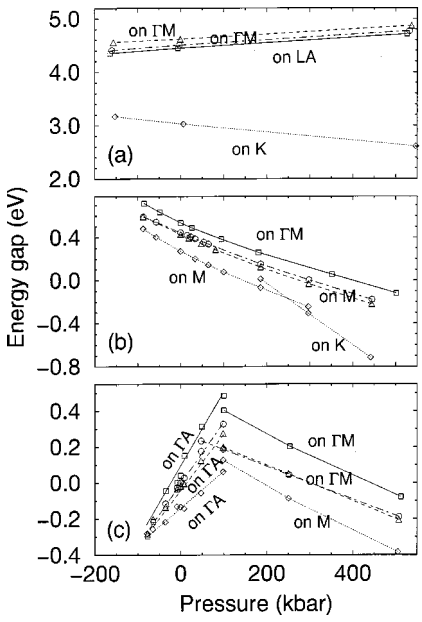

FIG. 9. Minimum energy gap vs pressure for the four polytypes of C (a), Si (b), and Ge (c). The position of the conduction-band minimum in **k** space is indicated. $3C$: squares, solid lines. $6H$: circles, dot-dashed lines. $4H$: triangles, dashed lines. $2H$: diamonds, dotted lines.

The pressure dependence of the fundamental gap of each polytype is displayed in Fig. 9. The changes versus pressure in the **k**-space location of the conduction-band minimum for germanium and $2H$-Si are also indicated. The pressure dependence of the transition energies depends very much on the group-IV element. It is almost weak or even vanishing for the carbon polytypes. There the gaps are opened when applying hydrostatic pressure. The only exception concerns the indirect ΓK gap in $2H$-C that is closed under pressure, in agreement with calculations from Fahy and Louie[52] (cf. Table IV). For silicon, the pressure coefficients exhibit clear trends with hexagonality. On an absolute scale, they decrease with increasing hexagonality. However, the sign of the pressure coefficients of the indirect gaps ΓM and ΓK is different

from that of the direct $\Gamma\Gamma$ gaps. The direct gaps are opened in the presence of pressure, whereas the indirect ones become smaller. The Ge polytypes show a similar behavior. Because of the different signs of the pressure coefficients, the energetical ordering of the conduction-band minimum is even changed under pressure [Fig. 9(c)]. The minimum of the conduction band is located on the ΓA line for a pressure lower than 100 kbar and on the ΓM line for a larger pressure.

IV. CONCLUSIONS

In summary, we have presented extensive first-principles studies of the structural, energetical, and electronic properties of the hexagonal polytypes $2H$, $4H$, and $6H$ of the group-IV elements C, Si, and Ge. The structural optimizations taking into account all the degrees of freedom related to internal-cell positions give lattice constants of $4H$-C, $2H$-C, $2H$-Si, and $2H$-Ge in agreement with measured values. We observe a clear trend with the hexagonality of the polytype. In contrast, the averaged elastic properties represented by the bulk modulus and its pressure derivative vary only weakly with the polytype.

The studies of the energetical stability show rather surprising results. As is well known, the cubic polytype $3C$ is the most stable one for the group-IV elements. The total energy of the other polytypes increases with increasing hexagonality. However, no clear chemical trend with the atomic radius or the atomic number has been observed. From the thermodynamical point of view, the probability to prepare a hexagonal polytype, in particular $4H$ or $6H$, is the highest for silicon. We pointed out the important role of strain in the formation of hexagonal polytypes, at least for Si and Ge. Under hydrostatic pressure, there is a significant tendency to support the formation of hexagonal polytypes. The two tendencies are underlined by the formation energies of stacking faults in the diamond structure and their pressure dependence.

The different bond stacking in the polytypes remarkably influences the electronic properties. We predicted significant differences in the band structures between the hexagonal polytypes and the diamond structure. The fundamental energy gap decreases with increasing hexagonality of the polytype. This trend is opposite to that observed for SiC. Except for Ge with interpretation problems due to the calculational method used, the polytypes of C and Si have been found to be indirect semiconductors. The conduction-band minimum is usually located at or near the M point in the hexagonal Brillouin zone. However, for wurtzite carbon, the minimum is found at K, as in SiC. This tendency is reinforced under pressure. In the high-pressure limit, the lowest conduction band of $2H$-Si is also at K.

ACKNOWLEDGMENTS

Grants of computer time from the John von Neumann-Institute Jülich are acknowledged. The work was financially supported by the EU Research Training Network NANOPHASE (HPRN-CT-2000-00167).

[1] J.Z. Hu, L.D. Merkle, C.S. Menoni, and I.L. Spain, Phys. Rev. B **34**, 4679 (1986).
[2] M.T. Yin and M.L. Cohen, Phys. Rev. B **26**, 5668 (1982).
[3] R.J. Needs and A. Mujica, Phys. Rev. B **51**, 9652 (1995).
[4] A. Mujica, S. Radescu, A. Munoz, and R.J. Needs, Phys. Status Solidi B **223**, 379 (2001).
[5] C.J. Ackland, Phys. Status Solidi B **223**, 361 (2001).
[6] K. Takemura, U. Schwarz, K. Syassen, N.E. Christensen, M. Hanfand, D.L. Novikov, and I. Loa, Phys. Status Solidi B **223**, 385 (2001).
[7] K.E. Spear, A.W. Phelps, and W.B. White, J. Mater. Res. **5**, 2277 (1990).
[8] C.E. Holcombe, Calculated XRD Data for Polymorphic Forms of Carbon, Oak Ridge Y-12 Plant Report Y-1887 (1973).
[9] A.R. Verma and P. Krishna, *Polymorphism and Polytypism in Crystals* (Wiley, New York 1966).
[10] R.S. Ramsdell, Am. Mineral. **32**, 64 (1947).
[11] N.W. Jepps and T.F. Page, Prog. Cryst. Growth Charact. **7**, 259 (1983).
[12] R.H. Wentorf and J.S. Kasper, Science **139**, 238 (1962).
[13] V.G. Eremenko and V.I. Nikitenko, Phys. Status Solidi A **14**, 317 (1972).
[14] P. Pirouz, J. Yang, F. Ernst, and H.-J. Möller, in *High Resolution Microscopy of Materials*, edited by W. Krakow, F.A. Ponce, and D. J. Smith, Mater. Res. Soc. Symp. Proc. No. 139 (Materials Research Society, Pittsburgh, 1989), p. 199; P. Pirouz, R. Chaim, U. Dahmen, and K.H. Westmacott, Acta Metall. Mater. **38**, 313 (1990); U. Dahmen, K.H. Westmacott, P. Pirouz, and R. Chaim, *ibid.* **38**, 3273 (1990); P. Pirouz, U. Dahmen, K.H. Westmacott, and R. Chaim, *ibid.* **38**, 329 (1990).
[15] T.Y. Tan, H. Föll, and S.M. Hu, Philos. Mag. A **44**, 127 (1981).
[16] J.H. Kim and J.Y. Lee, Mater. Lett. **27**, 275 (1996); Thin Solid Films **292**, 313 (1997).
[17] Y. Zhang, Z. Iqbal, S. Vijayalakshmi, and H. Grebel, Appl. Phys. Lett. **75**, 2758 (1999).
[18] J.Y. Zhang, H. Ono, K. Uchida, S. Nozaki, and H. Morisaki, Phys. Status Solidi B **223**, 41 (2001).
[19] M. Hendriks, S. Radelaar, A.M. Beers, and J. Bloem, Thin Solid Films **113**, 59 (1984).
[20] H. Cerva, J. Mater. Res. **6**, 2324 (1991).
[21] S.-Q. Xiao and P. Pirouz, J. Mater. Res. **7**, 1407 (1992).
[22] P. Pirouz, A. Garg, X.J. Ning, J.W. Yang, and S.Q. Xiao, in *Mechanical Behavior of Diamond and Other Forms of Carbon*, edited by M.D. Drory, M.S. Donley, D. Bogy, and J.E. Field, Mater. Res. Soc. Symp. Proc. No. **383** (Materials Research Society, Pittsburgh, 1995) 73.
[23] P. Müllner and P. Pirouz, Mater. Sci. Eng., A **233**, 139 (1997).
[24] U. Kaiser, A. Chüvilin, and W. Richter, J. Electron Microsc. **50**, 251 (2001).
[25] C. Schubert, W. Wesch, U. Kaiser, T. Gorelik, U. Glatzel, A. Hedler, J. Kräusslich, and K. Goetz, J. Appl. Phys. **91**, 3 (2002).
[26] E. Lopez-Cruz and M. Cardona, Solid State Commun. **45**, 787 (1983).

[27] R.E. Hanneman, H.M. Strong, and F.P. Bundy, Science **155**, 955 (1967).
[28] F.P. Bundy and J.S. Kasper, J. Chem. Phys. **46**, 4737 (1967).
[29] J. Glass, Bull. Am. Phys. Soc. **34**, 945 (1989).
[30] M. Frenklach, R. Kematick, D. Huang, W. Howard, K.E. Spear, A.W. Phelps, and R. Koba, J. Appl. Phys. **66**, 395 (1989).
[31] A.K. Sharma, H.G. Salunke, G.P. Das, P. Ayyub, and M.S. Multani, J. Phys.: Condens. Matter **8**, 5801 (1996).
[32] G.W. Yang and J.B. Wang, Appl. Phys. A: Mater. Sci. Process. **72**, 475 (2001).
[33] J.M. Besson, E.H. Mokhtari, J. Gonzalez, and G. Weill, Phys. Rev. Lett. **59**, 473 (1987).
[34] R.J. Kobliska and S.A. Solin, Phys. Rev. B **8**, 3799 (1973).
[35] M.R. Salehpour and S. Satpathy, Phys. Rev. B **41**, 3048 (1990).
[36] P. Hohenberg and W. Kohn, Phys. Rev. **136**, B864 (1964).
[37] W. Kohn and L.J. Sham, Phys. Rev. **140**, A1133 (1965).
[38] J.D. Joannopoulos and M.L. Cohen, Phys. Rev. B **7**, 2644 (1973); **8**, 2733 (1973).
[39] M. Murayama and T. Nakayama, Phys. Rev. B **49**, 4710 (1994).
[40] C.-Y. Yeh, Z.W. Lu, S. Froyen, and A. Zunger, Phys. Rev. B **46**, 10 086 (1992).
[41] J. von Boehm and P. Bak, Phys. Rev. Lett. **42**, 122 (1979).
[42] G. Kresse and J. Furthmüller, Comput. Mater. Sci. **6**, 15 (1996); Phys. Rev. B **54**, 11 169 (1996).
[43] J. Furthmüller, P. Käckell, F. Bechstedt, and G. Kresse, Phys. Rev. B **61**, 4576 (2000).
[44] S.G. Louie, S. Froyen, and M.L. Cohen, Phys. Rev. B **26**, 1738 (1982).
[45] J.P. Perdew and A. Zunger, Phys. Rev. B **23**, 5048 (1981).
[46] H.J. Monkhorst and J.K. Pack, Phys. Rev. B **13**, 5188 (1976).
[47] P. Käckell, B. Wenzien, and F. Bechstedt, Phys. Rev. B **50**, 17 037 (1994).
[48] F. Bechstedt, P. Käckell, A. Zywietz, K. Karch, B. Adolph, K. Tenelsen, and J. Furthmüller, Phys. Status Solidi B **202**, 35 (1997).
[49] P. Vinet, J. Ferrante, J.R. Smith, and J.H. Rose, J. Phys. C **19**, L467 (1986).
[50] J.-M. Wagner and F. Bechstedt, Phys. Rev. B **62**, 4526 (2000).
[51] *Numerical Data and Functional Relationships in Science and Technology*, Crystal and Solid State Physics, edited by O. Madelung and M. Schulz, Landolt-Börnstein, New Series, Group III, Vol. 22, Pt. a (Springer-Verlag, Berlin, 1987).
[52] S. Fahy and S.G. Louie, Phys. Rev. B **36**, 3373 (1987).
[53] B. Farid and R.J. Needs, Phys. Rev. B **45**, 1067 (1992).
[54] F. Bechstedt, U. Grossner, and J. Furthmüller, Phys. Rev. B **62**, 8003 (2000).
[55] A. Bauer, J. Kräusslich, L. Dressler, P. Kuschnerus, J. Wolf, K. Goetz, P. Käckell, J. Furthmüller, and F. Bechstedt, Phys. Rev. B **57**, 2647 (1998).
[56] C. Raffy, Ph.D. thesis, INP Grenoble, France, 2000.
[57] R. Biswas, R.M. Martin, R.J. Needs, and O.H. Nielsen, Phys. Rev. B **35**, 9559 (1987).
[58] A. Kailer, Y.G. Gogotsi, and K.G. Nickel, J. Appl. Phys. **81**, 3057 (1997).
[59] H. Olijnyk and A.P. Jephcoat, Phys. Status Solidi B **211**, 413 (1999).
[60] C. Cheng, R.J. Needs, and V. Heine, J. Phys. C **21**, 1049 (1988).
[61] S. Limpijumnong and W.R.L. Lambrecht, Phys. Rev. B **57**, 12 017 (1998).
[62] P.J.H. Denteneer, in *Atomic Scale Calculations in Materials Science*, edited by J. Tersoff, D. Vanderbilt, and V. Vitek, Mater. Res. Soc. Symp. Proc. No. 141 (Materials Research Society, Pittsburgh, 1989), p. 343.
[63] M.Y. Chou, M.L. Cohen, and S.G. Louie, Phys. Rev. B **32**, 7979 (1985).
[64] A. Gross and H. Teichler, Philos. Mag. B **64**, 413 (1991).
[65] P. Käckell, J. Furthmüller, and F. Bechstedt, Phys. Rev. B **58**, 1326 (1998).
[66] L.F. Mattheiss and J.R. Patel, Phys. Rev. B **23**, 5384 (1981).
[67] H. Föll and C. Carter, Philos. Mag. A **40**, 497 (1979).
[68] P. Pirouz, D.J.H. Cockayne, N. Sumida, P. Hirsch, and A.R. Lang, Proc. R. Soc. London, Ser. A **386**, 241 (1983).
[69] M.S. Hybertsen and S.G. Louie, Phys. Rev. B **34**, 5390 (1986).
[70] F. Bechstedt, Adv. Solid State Phys. **32**, 161 (1992).
[71] C. Herring, J. Franklin Inst. **233**, 525 (1942).
[72] P. Käckell, B. Wenzien, and F. Bechstedt, Phys. Rev. B **50**, 10 761 (1994).
[73] W.R.L. Lambrecht, S. Limpijumnong, S. Rashkeev, and B. Segall, Phys. Status Solidi B **202**, 5 (1997).